telecom

MDPI

Article

Reliable and Resilient Wireless Communications in IoT-Based Smart Agriculture: A Case Study of Radio Wave Propagation in a Corn Field

Blagovest Nikolaev Atanasov [1,*], Nikolay Todorov Atanasov [2] and Gabriela Lachezarova Atanasova [2]

[1] Faculty of Telecommunications, Technical University of Sofia, 1000 Sofia, Bulgaria
[2] Department of Communication and Computer Engineering, South-West University "Neofit Rilski", 2700 Blagoevgrad, Bulgaria; natanasov@swu.bg (N.T.A.); gatanasova@swu.bg (G.L.A.)
* Correspondence: b_atanasov@outlook.com

Abstract: In the past few years, one of the largest industries in the world, the agriculture sector, has faced many challenges, such as climate change and the depletion of limited natural resources. Smart Agriculture, based on IoT, is considered a transformative force that will play a crucial role in the further advancement of the agri-food sector. Furthermore, in IoT-based Smart Agriculture systems, radio wave propagation faces unique challenges (such as attenuation in vegetation and soil and multiple reflections) because of sensor nodes deployed in agriculture fields at or slightly above the ground level. In our study, we present, for the first time, several models (Multi-slope, Weissberger, and COST-235) suitable for planning radio coverage in a cornfield for Smart Agriculture applications. We received signal level measurements as a function of distance in a corn field (R3 corn stage) at 0.9 GHz and 2.4 GHz using two transmitting and two receiving antenna heights, with both horizontal and vertical polarization. The results indicate that radio wave propagation in a corn field is influenced not only by the surrounding environment (i.e., corn), but also by the antenna polarization and the positions of the transmitting and receiving antennas relative to the ground.

Keywords: IoT; radio wave propagation; precision agriculture; smart agriculture; attenuation in vegetation and soil; near-ground propagation; above-ground propagation; wireless communications

Citation: Atanasov, B.N.; Atanasov, N.T.; Atanasova, G.L. Reliable and Resilient Wireless Communications in IoT-Based Smart Agriculture: A Case Study of Radio Wave Propagation in a Corn Field. *Telecom* **2024**, *5*, 1161–1178. https://doi.org/10.3390/telecom5040058

Academic Editor: Petros Bithas

Received: 13 September 2024
Revised: 15 October 2024
Accepted: 6 November 2024
Published: 12 November 2024

1. Introduction

In the past few years, one of the largest industries in the world, the agriculture sector, has faced many challenges, such as providing more and better food due to the exponential growth of the world population (from 1.65 billion in 1900 to 10.1 billion in 2050 [1–4]), climate change (by affecting the crop production by 2030 [5,6]), and the depletion of limited natural resources. Precision agriculture (PA), also known as smart agriculture, based on the Internet of Things (IoT), is seen as a transforming force that will play a vital role in the further development of agriculture in the coming decades [7–9]. Smart agriculture uses cutting-edge technologies (such as IoT, 5G and wireless sensor networks (WSNs)) for real-time monitoring of plant growth and health and environment parameters aiming to improve crop production, while at the same time conserving natural resources and reducing greenhouse gas emissions [10–14]. For example, with real-time data on soil moisture levels, temperature, pH, and humidity, farmers can reduce the risk of crop diseases and root rot, as well as prevent waterlogging and soil compaction. Plant disease diagnosis is another area where real-time monitoring offers significant benefits. For instance, biosensors enable the early detection of airborne pathogens, allowing farmers to take quick action and minimize crop losses. IoT-based real-time data collection requires deploying many sensor nodes in vegetation fields that are spatially distributed and interconnected wirelessly. Each node consists of a sensor, a microcontroller for signal processing, a transceiver with an antenna, and a source of energy such as a battery or energy harvester (solar power or radio

frequency wave energy) [15–17]. The sensor nodes are connected to a server through a gateway (base station) to exchange, process, and store the collected data using the Internet environment [17–19]. For supporting real-time data flow in such networks, it is essential to ensure a reliable and resilient wireless connection between the nodes (sensor(s) and gateway) [20], as the dynamics of the radio channel directly impact data loss and delay during node-to-node data exchange [21–23]. Furthermore, in IoT-based smart agriculture systems, radio wave propagation faces unique challenges (such as attenuation in vegetation and soil and multiple reflections) because of sensor nodes deployed in agriculture fields at or slightly above the ground level. For instance, to gather real-time data on soil moisture levels, temperature, pH, etc., the communication nodes should be positioned in rows alongside the crop on the ground or elevated up to 0.5 m above ground to reduce the risk of node damage by tractors and implements. Hence, there is a need for extensive measurement companies to study radio wave propagation in vegetation fields and find the model(s) that best represent the propagation characteristics in the communication scenarios of smart agriculture.

Pioneering measurements were conducted at 2.4 GHz to study radio wave propagation in corn fields [22,24,25]. A distance from 70 m up to 100 m was defined as a stable communication distance between the sensor node and the base station at 2.4 GHz at a fixed base station antenna height (1 m, 2 m, and 3 m) [22] and in obstructed line-of-sight (O-LoS) scenarios, i.e., vegetation between Tx-Rx in LoS. Moreover, in most previous studies of radio wave propagation in vegetation environments, the antenna of the sensor node (i.e., antenna in the vegetation field) has been placed between 0.9 m and 3 m [22,24,26,27] above the ground. However, this placement does not allow for a proper evaluation of the actual characteristics of wireless channels for real Smart Agriculture scenarios for near-ground communications [28]. Moreover, to achieve an IoT-based system capable of supporting real-time data exchange for remote monitoring in precision agriculture, a variety of wireless communication standards and technologies for IoT applications, including the SigFox (0.868–0.869 GHz and 0.902–0.928 GHz), LoRaWAN (Long Range Wide Area Network) (0.867–0.869 GHz and 0.902–0.928 GHz), Narrowband-Internet of Things (NB-IoT) (B3, B8, and B20), ZigBee (0.867, 0.914 GHz), and Bluetooth (2.4–2.4835 GHz), have been proposed [14,29–34].

In this paper, we present, for the first time, several models (Multi-slope, Weissberger, and COST-235) suitable for planning radio coverage in a corn field for smart agriculture applications. Radio wave propagation measurements for real smart agriculture scenarios in a corn field at two different frequencies (0.9 GHz and 2.4 GHz) using reference dipoles are presented. The dipole within the corn field was located at one-third of the wavelength (0.11 m and 0.04 m at 0.9 GHz and 2.4 GHz, respectively) and 0.5 m above ground to represent near-ground and above-ground propagation. In addition, we present path loss at 0.9 GHz and 2.4 GHz under the two transmitting and two receiving antenna heights at horizontal and vertical polarization based on the measurement data in the corn field. Finally, we compare the measured path loss to the different propagation models to find the model(s) that best represent the propagation characteristics of various communication scenarios of smart agriculture in a corn field.

2. Radio Wave Propagation Measurements in a Corn Field

2.1. Measurement Environment

We conducted measurements in a corn field in an agricultural area (Figure 1) near Dabravata Village, Yablanitsa Municipality, Bulgaria, in the summer of 2024 at the corn reproductive (R3) stage. It is important to note that, from emergence (VE) to physiological maturity (R6), corn growth is divided into two key stages—the vegetative (V) and reproductive (R) stages. The corn plant reaches full height, and all leaves emerge at the end of the vegetative growth stage. The reproductive stages begin at silking (R1) and at the end at maturity or "black layer" (R6). Plants at R2 have reached their maximum height, and the kernel size is rapidly increasing. At stages R3, R4, R5, and R6, the kernels'

moisture content is approximately 80%, 70%, 55%, and 30–35%, respectively [35–37]. We chose to observe the radio wave propagation at stage R3 (known as the milk growth stage due to the milky white fluid in the kernel) because, at this stage, the leaves and stalk almost do not change, the kernels contain approximately 80% moisture, and starch starts to accumulate within them [35–37]. Moreover, in stage R3, we expect the highest signal attenuation due to the highest density of leaf and kernel moisture in this stage. In the chosen agricultural field for the experiment, the corn was planted in rows with a row spacing of 0.70 ± 0.05 m. The distance between individual corn plants within each row was 0.20 ± 0.03 m. The average number of plants per hectare was 70,000. The average height of the corn plants was 2.6 ± 0.2 m, and the average leaf number was 12 ± 1. We chose to study radio wave propagation in the corn field because corn is one of the most widely produced crops globally [38,39], making it an excellent choice for implementing smart agriculture.

(**a**) (**b**)

Figure 1. Measurements in a corn field in the agricultural area near Dabravata Village, Yablanitsa Municipality, Bulgaria: (**a**) Google Earth image; (**b**) photo from the corn field.

2.2. Measurement Equipment and Setup

Figure 2 shows the configuration of the measurement setup consisting of a portable RF signal generator (AS108, Pico Technology, Tyler, TX, USA, frequency range 300 kHz–8 GHz) directly connected to a reference dipole. The RF generator was configured to generate a continuous wave (CW) signal with a frequency of 0.9 GHz or 2.4 GHz and a power level of 0 dBm. The generator and the antenna were positioned in the corn field and relocated, as illustrated in Figure 3a,d. The transmitted CW signal was captured by a real-time spectrum analyzer (R5550-427, thinkRF, Ottawa, ON, Canada, frequency range 9 kHz–27 GHz) using a reference dipole antenna and stored on a laptop connected to the analyzer through an Ethernet interface for post-processing. The spectral analyzer and antenna were located outside the cornfield, as shown in Figure 3b. The coordinates of the receiving antenna are 43°05′19″ N 24°02′17″ E.

Figure 2. Configuration of the measurement setup.

Four reference dipoles with λ/4 parallel conductor balun using a 3.6 mm diameter semi-rigid cable were constructed according to IEC/IEEE 62209-1528:2020 Std. [40] to carry out the measurements. Two dipoles operated at 0.9 GHz and the other two at 2.4 GHz. The mechanical dimensions and $|S_{11}|$ of the dipoles are presented in Table 1. A vector network analyzer (Tektronix TTR503A, Tektronix, Inc., Beaverton, OR, USA) was used to measure S parameters. Before measurements, an Open-Short-Load calibration was performed.

Table 1. Mechanical dimensions and $|S_{11}|$ of the constructed reference dipoles.

Frequency *	Length of Dipole Arms **	Diameter of the Dipol **	Connector Type	$\|S_{11}\|$ at Operating Frequency
0.9	150	3.6	N	−15.1
2.4	52	3.6	N	−10.3

* The frequency indicated in the table is in GHz. ** The lengths and diameters in the table are in millimeters.

To study the near- and above-ground radio wave propagation in real-world smart agriculture scenarios, the transmitting (Tx) dipole antenna (more specifically its feed point) was positioned in the corn field at a distance from the ground equal to one-third of the wavelength (0.11 m and 0.04 m at 0.9 GHz and 2.4 GHz, respectively) and 0.5 m above the ground. We experimentally determined the minimum height for installing the Tx dipole above the soil by measuring the S_{11} parameters at different heights. It is well known that the proximity of the dipole to the ground can significantly impact the antenna's parameters and characteristics. Figure 4 displays the measured $|S_{11}|$ at a distance from the ground equal to one-third of the wavelength. The results show that placing the dipole at a distance less than 0.3λ m from the ground significantly affects antenna characteristics, including resonant frequency and input impedance, due to proximity effects.

The receiving (Rx) dipole antenna positioned outside the cornfield was at a height of 2.0 m and 3.4 m above the ground, as shown in Figure 3b,c. We selected 29 transmitter–receiver locations in obstructed line-of-sight (O-LoS) conditions to perform measurements for vertically and horizontally polarized antennas. Received signal levels (Rx Levels) from the spectrum analyzer were recorded at 1 m, 5 m, and every 5 m after that as the transmitter moved away from the receiver, resulting in 29 locations total for co-polarized vertical-to-vertical (V-V) antennas at both 0.9 GHz and 2.4 GHz. The procedure was repeated using co-polarized horizontal-to-horizontal (H-H) antennas. In addition, Tx and Rx antennas were located so that the line connecting the antennas was perpendicular to the corn rows, as depicted in Figure 3d. For each of the presented scenarios, ten consecutive values of the received signal level were measured for each location of the transmitting antenna. The graphs show the average values of the ten measurements.

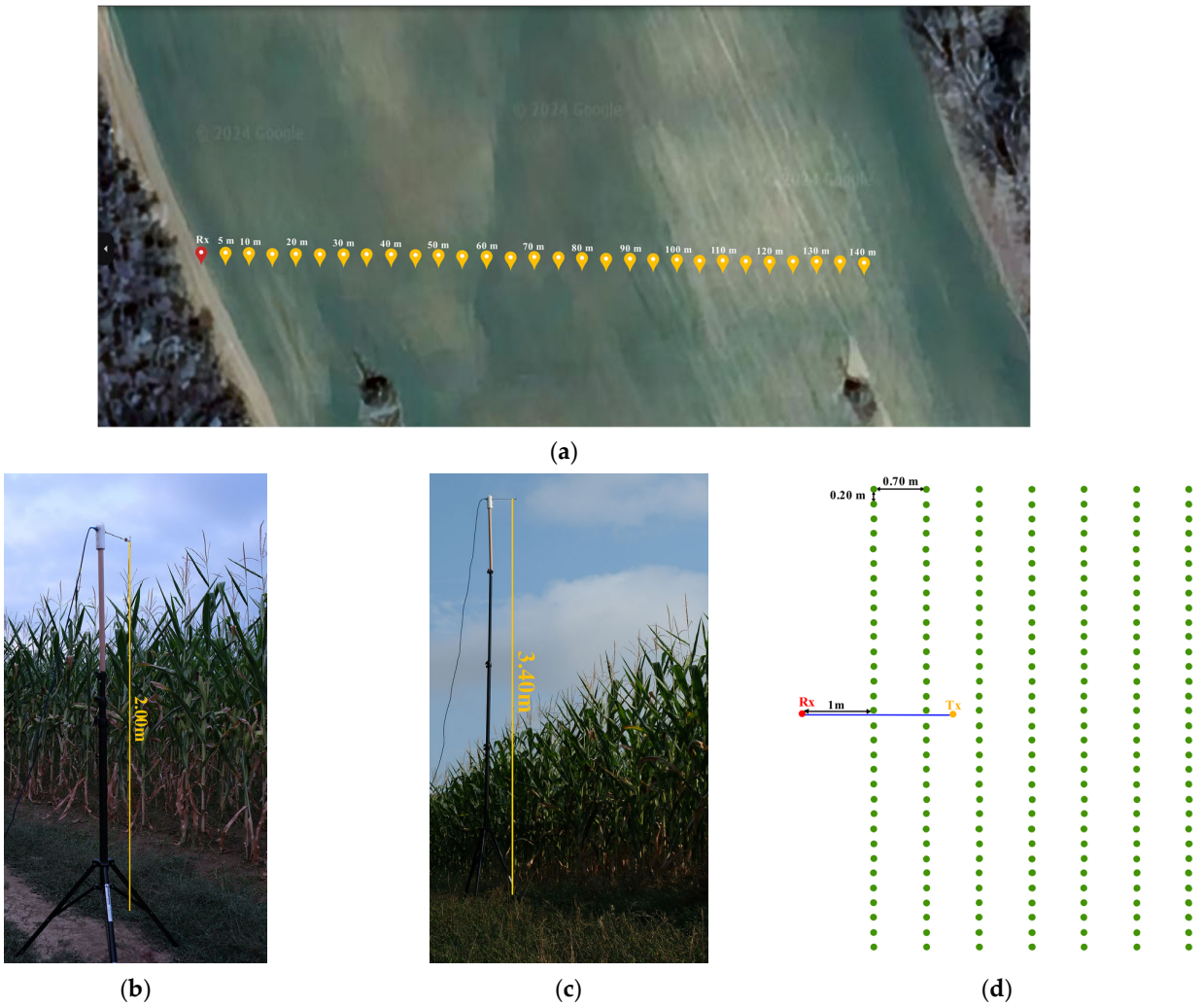

(**a**)

(**b**) (**c**) (**d**)

Figure 3. Measurement site: (**a**) Google Earth image with Tx and Rx antenna locations in the corn field; (**b**) photo of Rx antenna placed below the corn height; (**c**) photo of Rx antenna placed above the corn height; (**d**) direction of measurement at the experimental corn field.

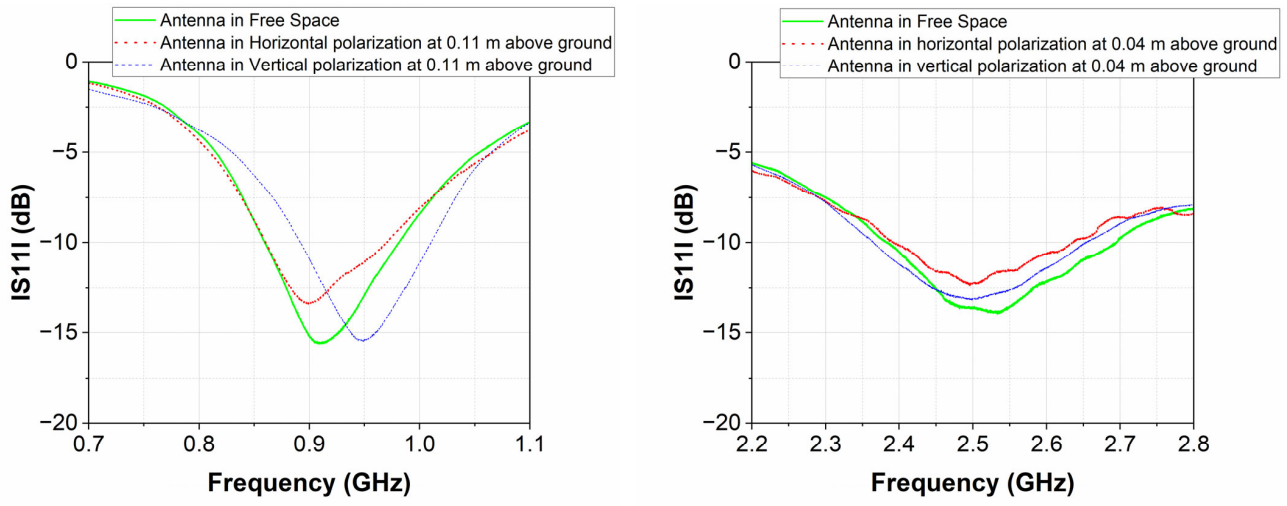

(**a**) (**b**)

Figure 4. Measured reflection coefficients for the two dipoles: (**a**) reference dipole used for measurements at 0.9 GHz; (**b**) reference dipole used for measurements at 2.4 GHz.

3. Results and Discussion

3.1. Measurement Results

In this subsection, we present the received signal level as a function of distance for measurements in a cornfield (R3 corn stage) at 0.9 GHz and 2.4 GHz under two transmitting and two receiving antenna heights at horizontal and vertical polarization.

Figures 5–8 show the received signal level variation with distance for the following scenarios: near-ground (transmitting antenna is placed at a height of λ/3 m above ground, h_{TX} = λ/3 m) and above-ground (transmitting antenna is placed at a height of 0.5 m above ground, h_{TX} = 0.5 m) installation of a sensor node in the corn field for two heights of the receiving antenna below (h_{Rx} = 2.0 m above ground) and above (h_{Rx} = 3.4 m above ground) corn height, at two frequencies of 0.9 GHz and 2.4 GHz for co-polarized horizontal-to-horizontal (H-H) and vertical-to-vertical (V-V) antennas. In all scenarios, the transmitter was positioned in the cornfield and relocated, as illustrated in Figure 3a.

In all scenarios under obstructed line-of-sight (O-LoS) conditions, the general trend was that the signal strength was reduced, with distance varying due to constructive and destructive interference. The peak signal strength at a receiving antenna height of 2 m occurred when the distance between the transmitting and receiving antennas was 1 m. At a receiving antenna height of 3.4 m (above the height of the corn), the peak signal strength occurred when the Tx-Rx distance was 5 m (see Figures 5 and 6).

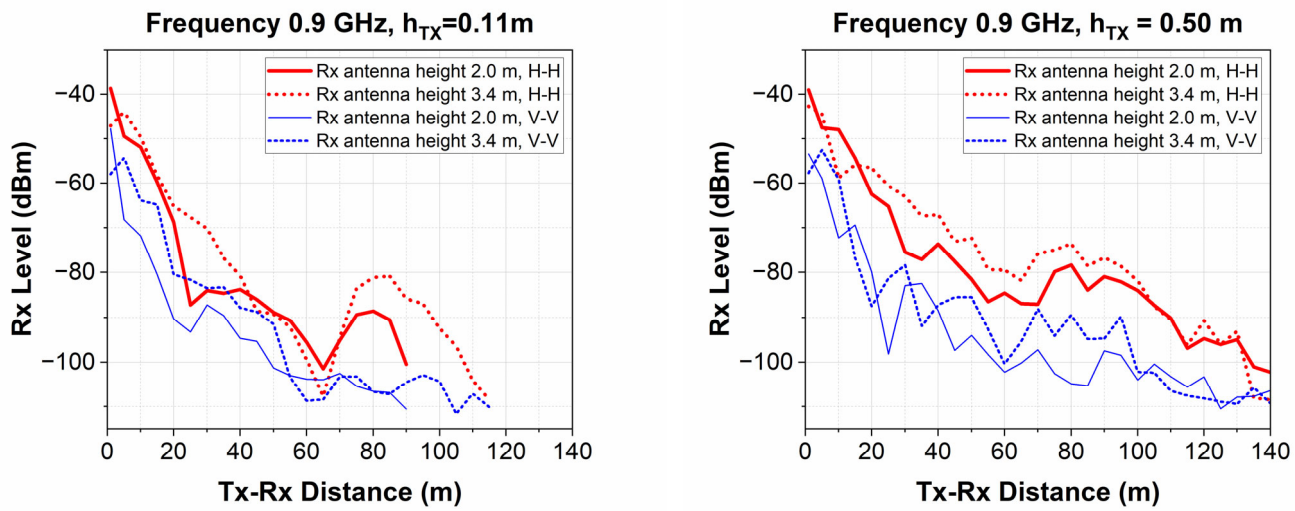

Figure 5. Received signal level variation with distance at 0.9 GHz for co-polarized H-H and V-V antennas: (**a**) transmitting antenna is placed at a height of λ/3 m above ground (hTx = 0.11 m); (**b**) transmitting antenna is placed at a height of 0.5 m above ground (hTx = 0.5 m).

Thus, we can see from Figures 5 and 6 that, when the receiving antenna height was below the corn height (h_{Rx} = 2.0 m), for H-H antennas at 0.9 GHz, the peak values of the received signal were −38.7 dBm (at h_{Tx} = 0.11 m) and −39.1 dBm (at h_{Tx} = 0.5 m), while at 2.4 GHz, the peak values of the received signal were −53.7 dBm (at h_{Tx} = 0.04 m) and −48.6 dBm (at h_{Tx} = 0.5 m). When comparing the curves shown in Figure 5 for H-H antennas at h_{Tx} = λ/3 m, it is evident that raising the receiving antenna above the corn (from 2.0 m to 3.4 m) reduced the oscillations in the received signal. This reduction occurred due to the decreased destructive interference at 0.9 GHz. This effect was less noticeable at h_{Tx} = 0.5 m (Figure 5b), as in the case of co-polarized vertical-to-vertical antennas. At 2.4 GHz, the height of the receiving antenna did not affect the received signal level when the transmitting antenna in the corn field was at a height of λ/3 m.

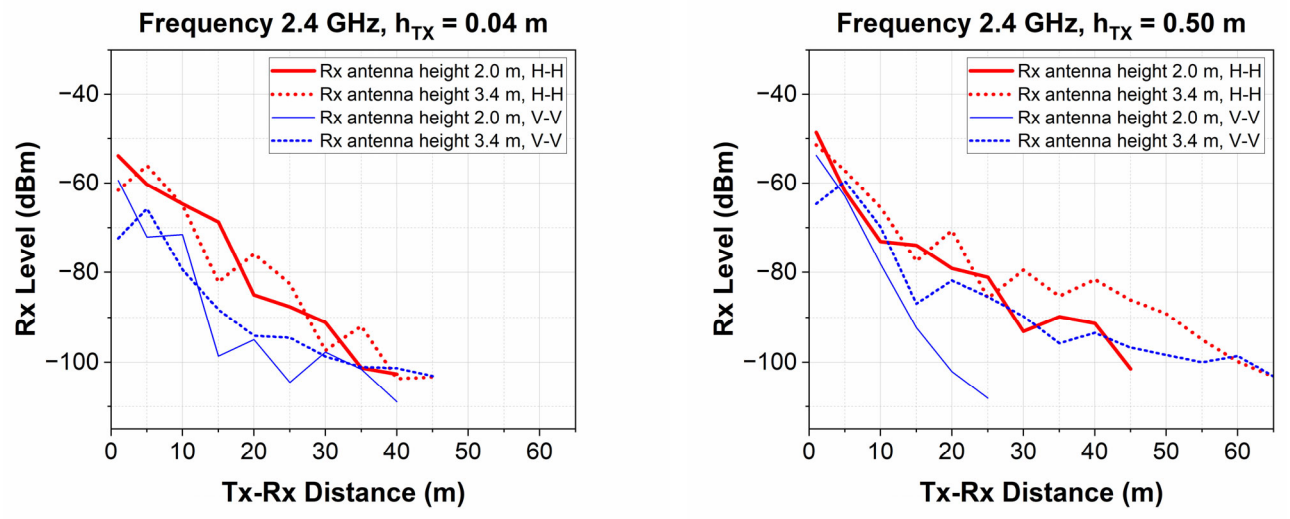

(**a**) (**b**)

Figure 6. Received signal level variation with distance at 2.4 GHz for co-polarized H-H and V-V antennas: (**a**) transmitting antenna is placed at a height of λ/3 m above ground (h_{Tx} = 0.04 m); (**b**) transmitting antenna is placed at a height of 0.5 m above ground (h_{Tx} = 0.5 m).

Figures 7 and 8 depict how the transmitting antenna height (sensor node antenna) influenced the received signal level and communication range. We observed that, at 0.9 GHz, H-H antennas, the receiving signal level increased, on average, by 8.7 dB (at h_{Rx} = 2.0, Figure 7a) and 9.6 dB (at h_{Rx} = 3.4, Figure 7b) after increasing the transmitting antenna height from 0.11 m to 0.5 m above ground. This effect was less noticeable at 2.4 GHz (Figure 8), as in the case of co-polarized vertical-to-vertical antennas (Figures 7 and 8). Comparing the curves in Figure 8, we can see that at 2.4 GHz, the received signal levels for transmitting antenna heights of 0.04 m and 0.5 m were nearly equal at a receiving antenna height of 2.0 m.

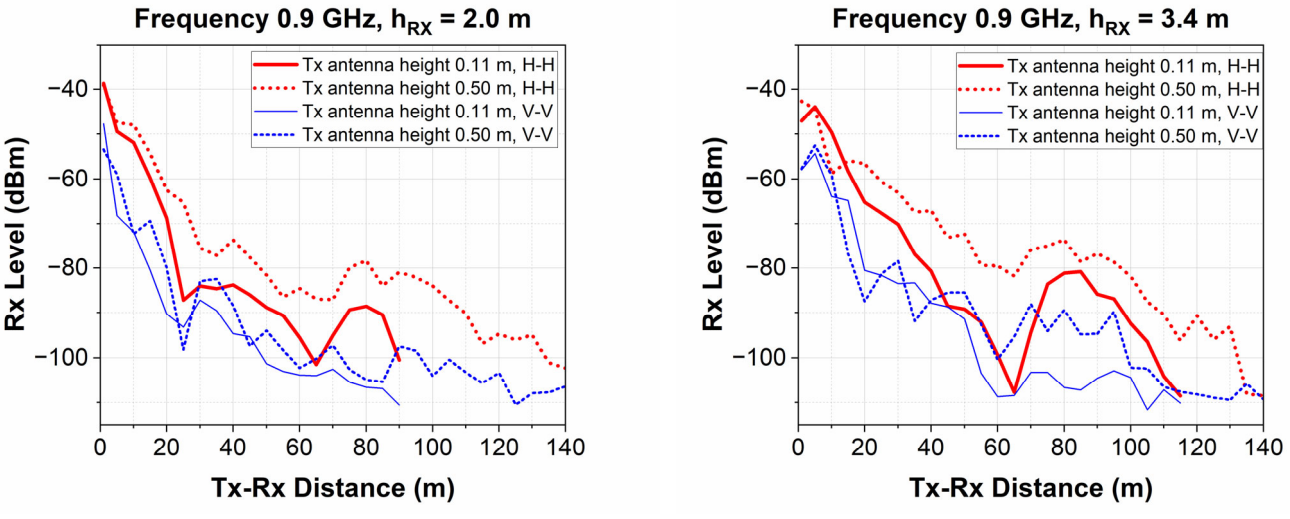

(**a**) (**b**)

Figure 7. Received signal level variation with distance at 0.9 GHz for co-polarized H-H and V-V antennas: (**a**) receiving antenna height below the corn height (h_{Rx} = 2.0 m); (**b**) receiving antenna height above the corn height (h_{Rx} = 3.4 m).

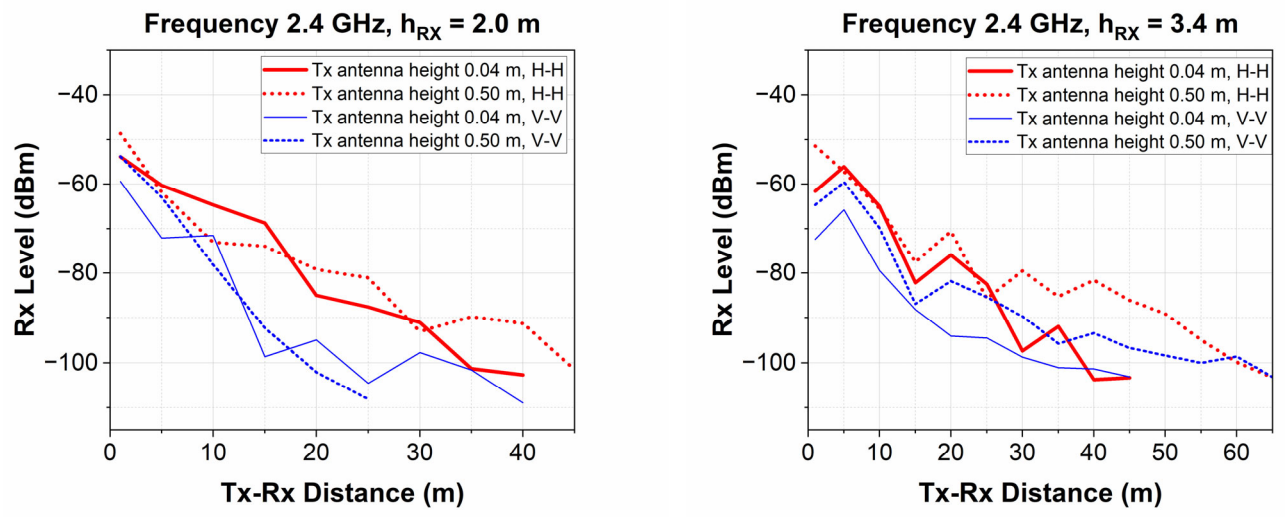

(**a**) (**b**)

Figure 8. Received signal level variation with distance at 2.4 GHz for co-polarized H-H and V-V antennas: (**a**) receiving antenna height below the corn height (h_{Rx} = 2.0 m); (**b**) receiving antenna height above the corn height (h_{Rx} = 3.4 m).

The results show that higher receiving levels were measured for co-polarized H-H antennas than for co-polarized V-V antennas for all scenarios in O-LoS conditions. The difference in the received signal level for vertical and horizontal polarization was due to the density of vegetation, its structure (leaves and stalks), and the water content [41], but predominantly (mainly) because in the corn field, the biomass was concentrated in the vertically oriented stalks planted in rows, as described in Section 2.1. For horizontally polarized waves, the electric field was perpendicular to the corn stalks. For vertically polarized waves, the electric field was parallel to the corn stalks, coupling strongly. By comparing the curves of Figure 5, we observe that at 0.9 GHz co-polarized H-H antennas, the receiving signal level increased, on average, by 12.5 dB (at h_{Tx} = 0.11 m, h_{Rx} = 2.0, Figure 5a), 11.6 dB (at h_{Tx} = 0.11 m, h_{Rx} = 3.4, Figure 5a), and 16 dB (at h_{Tx} = 0.5 m, h_{Rx} = 2.0 and h_{Rx} = 3.4, Figure 5b) in the same cases of co-polarized V-V antennas. From the results, we can conclude that at 0.9 GHz, the antenna polarization has an essential impact on the received signal level in the wireless sensor networks deployed in an agricultural environment for IoT-based smart agriculture.

From the obtained results (Figures 5–8) summarized in Tables 2 and 3, we can examine how the height of the transmitting and receiving antennas impacted the coverage area of a wireless sensor network for IoT-based smart agriculture. We assume that, for a reliable data connection between the sensor node (transmitter) and the gateway (receiver), the minimum received level should be −106 dBm (there would not be successful data transmission if the level fell below this threshold). Our analysis revealed that increasing the height of the receiving antenna above the corn height, from 2.0 m to 3.4 m, expanded the coverage area. Thus, at 0.9 GHz, for H-H antennas, with h_{Tx} = 0.11 m (h_{Tx} = λ/3 m) and an Rx antenna height of 3.4 m, the distance range was 105 m, whereas at an Rx antenna height of 2.0 m, it was 90 m. At 2.4 GHz, for H-H antennas, with h_{Tx} = 0.04 m (h_{Tx} = λ/3 m) and an Rx antenna height of 3.4 m, the communication distance range was 45 m, whereas at an Rx height of 2.0 m, it was 40 m. Also, we observed a more significant increase in the communication distance between the Tx-Rx antennas by increasing the transmitting antenna height from h_{Tx} = λ/3 (0.11 m at 0.9 GHz and 0.04 m at 2.4 GHz) to 0.5 m above ground level. Consequently, we can conclude that connectivity in a wireless sensor network for agriculture applications in a corn field is more sensitive to the sensor antenna's height from the ground than to the gateway antenna's height from the ground.

Based on the results presented in Tables 2 and 3, it is evident that at 0.9 GHz, the coverage radius (maximum communication distance) for sensors placed near the ground ($h_{Tx} = \lambda/3$ m) was less affected by antenna polarization compared to sensors positioned 0.5 m above the ground. Additionally, at 2.4 GHz, antenna polarization had minimal impact on the coverage area.

Table 2. Maximum communication distance between Tx and Rx at co-polarized H-H antennas.

Frequency *	Transmitting Antenna (Tx) Height **	Receiving Antenna (Rx) Height **	Maximum Communication Distance Between Tx and Rx **
0.9	0.11	2.0	90
	0.11	3.4	105
	0.50	2.0	140
	0.50	3.4	140
2.4	0.04	2.0	40
	0.04	3.4	45
	0.50	2.0	45
	0.50	3.4	65

* The frequency indicated in the table is in GHz. ** The antenna height and distance indicated in the table are in meters.

Table 3. Maximum communication distance between Tx and Rx at co-polarized V-V antennas.

Frequency *	Transmitting Antenna (Tx) Height **	Receiving Antenna (Rx) Height **	Maximum Communication Distance Between Tx and Rx **
0.9	0.11	2.0	80
	0.11	3.4	100
	0.50	2.0	120
	0.50	3.4	110
2.4	0.04	2.0	40
	0.04	3.4	45
	0.50	2.0	20
	0.50	3.4	65

* The frequency indicated in the table is in GHz. ** The antenna height and distance indicated in the table are in meters.

3.2. Model Selection and Application for Short-Range Propagation in a Corn Field

In this section, we present the propagation data and compare the measured path loss to different propagation models to find the model(s) that best represent the propagation characteristics in a corn field in several scenarios of smart agriculture applications.

Calculation of Path Loss

The measured path loss L_M in dB as a function of the distance (d) is computed using the following formula [42]:

$$L_M(d) = P_T + G_T + G_R - P_R(d), \quad (1)$$

where:

- P_T is the transmitted power (which remains constant $P_T = 0$ dBm);
- P_R (in dBm) is the received power, varying as a function of distance;
- G_T and G_R represent the gains of the transmitting and receiving reference dipole antennas, which are both 2.15 dBi.

Figures 9–12 show comparisons of the measured path loss for various scenarios, with predictions from two of the most commonly used models predicting the additional attenuation of a wireless link passing through vegetation—the Weissberger and COST-235 models [43,44]. These models are modified exponential decay models and have the generic form given by [45]:

$$L(f,d) = A \times F^B \times d^C, \quad (2)$$

where:

- L is attenuation loss in dB;
- F is the frequency in MHz or GHz;
- d is the depth of the vegetation along the line-of-sight path in meters;
- A, B, and C are model parameters. They are presented in Table 4.

Table 4. Basic input parameters values for Weissberger, COST-235, and Multi-slope models.

	Basic Input Parameters						
Model Names	**A**	**B**	**C**	n_1	n_2	**Frequency Units**	**Note**
Weissberger *	1.33	0.284	0.588	-	-	GHz	14 m $< d \leq$ 400 m
	0.45	0.284	-	-	-	GHz	0 m $< d <$ 14 m
COST-235 **	15.6	−0.009	0.26	-	-	MHz	in leaf
	26.6	−0.2	0.5	-	-	MHz	out of leaf
Multi-slope model	-	-	-	2.0	-	-	$d \leq d_{bp}$
	-	-	-	2.0	4.0	-	$d > d_{bp}$

* The range of frequencies for the Weissberger model is from 0.23 GHz to 9.2 GHz. ** The range of frequencies for the COST-235 model is from 9.6 GHz to 57.6 GHz.

The additional attenuation caused by vegetation for each model is added to the basic free-space loss to calculate the predicted path loss shown in Figures 9–12.

The basic free-space transmission loss (L_{bs}) in decibels (dB) is calculated by [46]:

$$L_{bs}(f,d) = 32.4 + 20\log F + 20\log d \quad (3)$$

where:

- F is the frequency in MHz;
- d is the distance in kilometers.

In the Weissberger and COST-235 models for transmission loss in the vegetation, the loss between antennas is expressed as the sum of free-space basic transmission loss, L_{bs}, and additional loss, L, such as foliage losses in crop or forestry scenarios [43]. In addition, in the modified exponential decay models, L_{bs} and L are frequency- and distance-dependent and independent of the antenna height.

Furthermore, the results presented in Figures 5–8 and Tables 2 and 3 in Section 3.1 indicate that radio wave propagation in the corn field is impacted not only by the surrounding environment (i.e., corn), but also by the positions of the transmitting and receiving antennas relative to the ground. Hence, to include the effects of the antenna height, we compare the results with the multi-slope model (two slopes and a single breakpoint). In the model, the path loss, L, is assumed to increase with a given slope up to a 'breakpoint'. Beyond this point, the slope becomes steeper. The L in dB is given by [42]:

$$L(d) = \begin{cases} 10n_1 \log d + L_1, & d \leq d_{bp} \\ 10n_2 \log\left(\frac{d}{d_{bp}}\right) + 10n_1 \log d_{bp} + L_{1,} & d > d_{bp} \end{cases} \quad (4)$$

where:

- L_1 is a value for the basic transmission loss at the d = 1 m;
- d is the distance in meters;
- d_{bp} is the breakpoint distance in meters and is given by:

$$d_{bp} = (4h_{Tx}h_{Rx})/\lambda, \quad (5)$$

where:

- λ is the wavelength in meters;
- h_{Tx} is transmitting antenna height in meters;

- h_{Rx} is receiving antenna height in meters;
- n_1 and n_2 are model parameters. They are presented in Table 4.

For each data set (communication scenario in corn field) and each model, we present in Tables 5 and 6 the mean absolute percentage error (MAPE), in %, to compare the prediction accuracies of the path loss models. The MAPE is given by:

$$\text{MAPE} = \frac{100}{n}\sum_{i=1}^{n}\frac{|L_{Mi}-L_{MODELi}|}{L_{Mi}} \quad (6)$$

where:

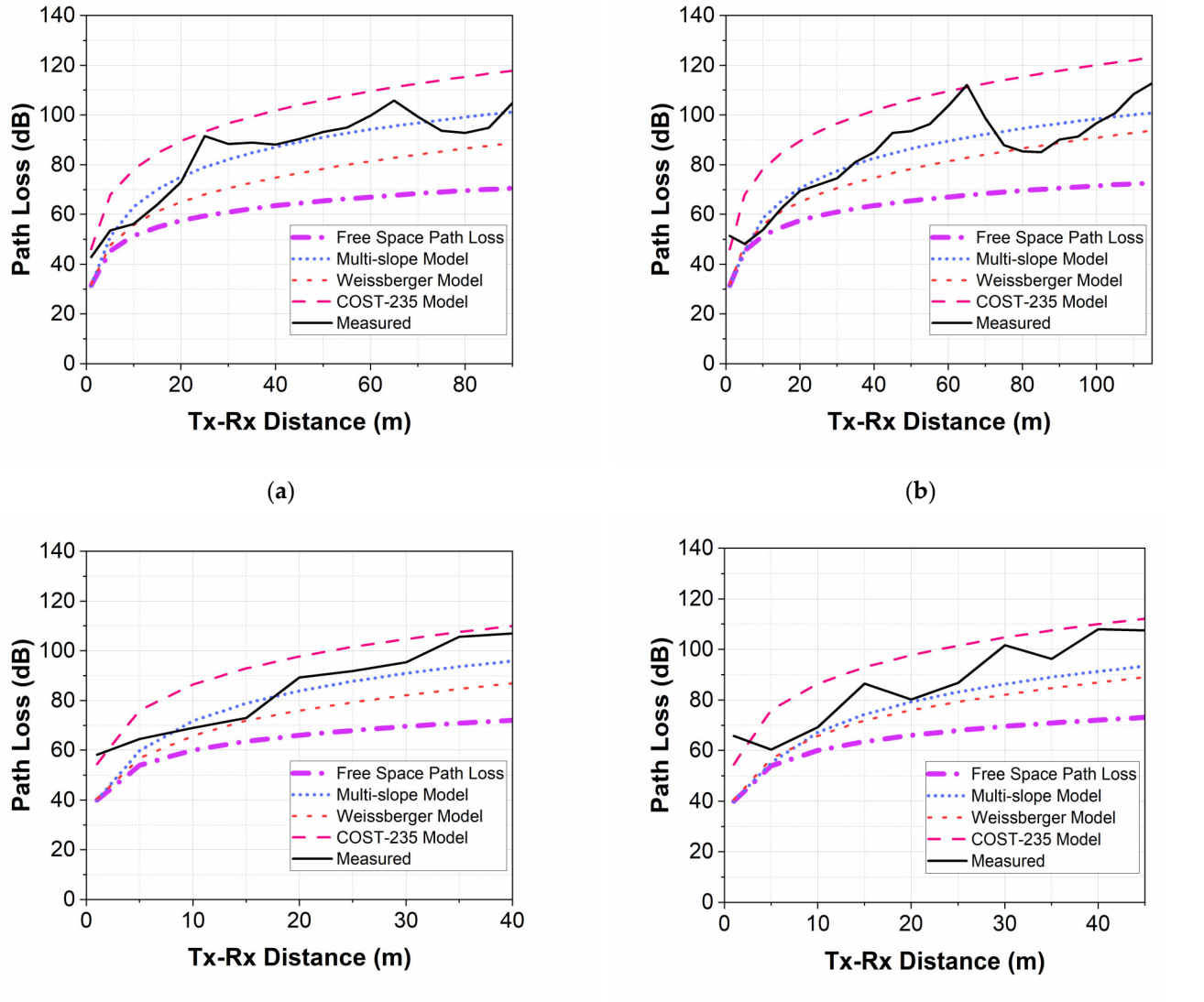

Figure 9. Comparison between losses for co-polarized H-H antennas at transmitting antenna height λ/3 m with existing models: (**a**) 0.9 GHz, h_{Rx} = 2.0 m; (**b**) 0.9 GHz, h_{Rx} = 3.4 m; (**c**) 2.4 GHz, h_{Rx} = 2.0 m; (**d**) 2.4 GHz, h_{Rx} = 3.4 m.

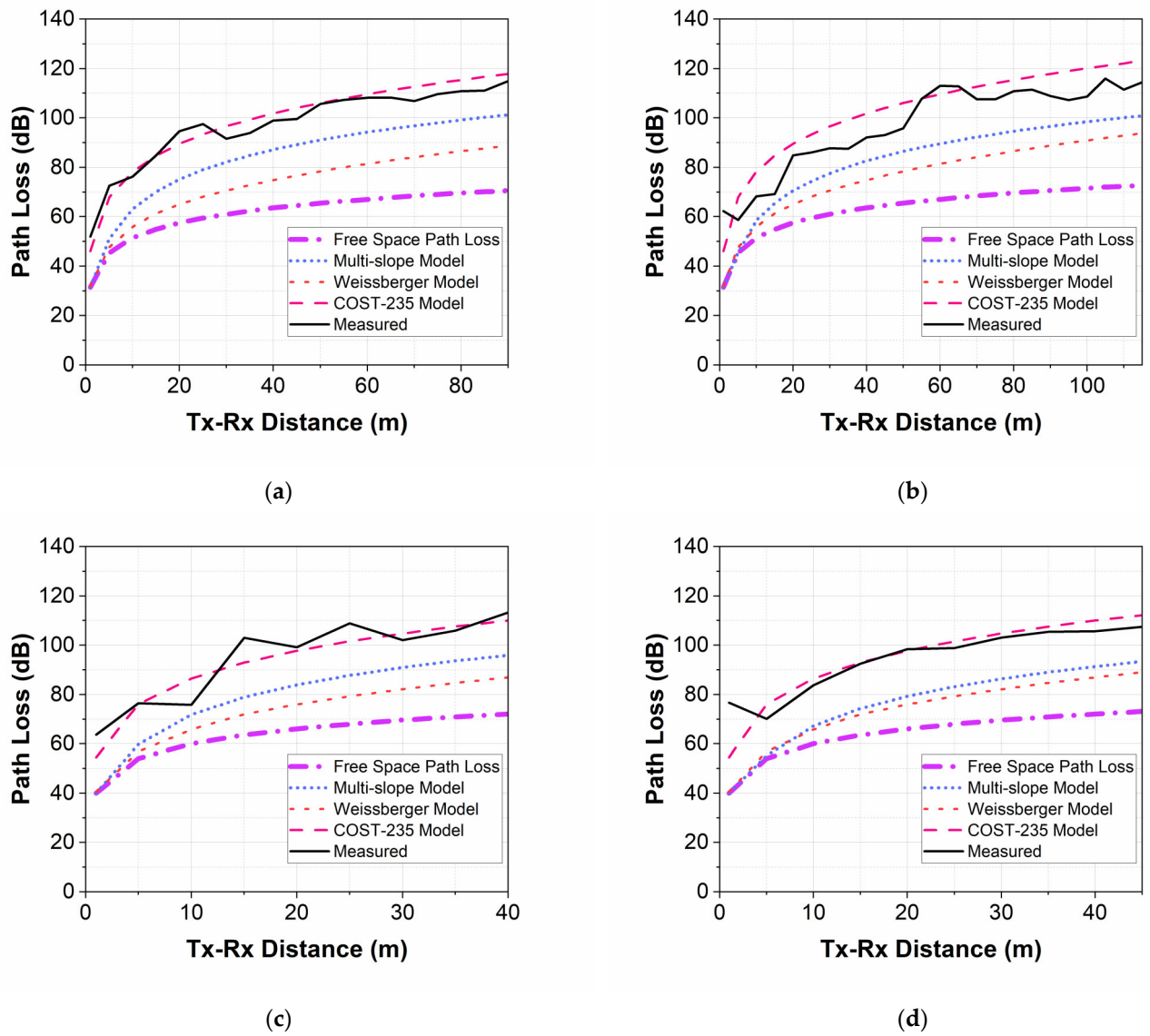

Figure 10. Comparison between losses for co-polarized V-V antennas at transmitting antenna height λ/3 m with existing models: (**a**) 0.9 GHz, h_{Rx} = 2.0 m; (**b**) 0.9 GHz, h_{Rx} = 3.4 m; (**c**) 2.4 GHz, h_{Rx} = 2.0 m; (**d**) 2.4 GHz, h_{Rx} = 3.4 m.

- *n* is the number of measurements;
- L_M and L_{MODEL} represent measured and predicted path loss, respectively, and *i* is the index of each sample.

Figures 9 and 10 illustrate the comparison between predictions of the Weissberger, COST-235, and Multi-slope models and measured losses at the near-ground installation of the sensor node in the corn field, i.e., for transmitting antenna height λ/3 m at two frequencies (0.9 GHz and 2.4 GHz) and two receiving antenna heights (2.0 m and 3.4 m) for H-H (Figure 9) and V-V (Figure 10) polarized antennas. From Figure 9 and Tables 5 and 6, we can observe that, when using co-polarized H-H antennas for near-ground sensor node installation in a corn field, the COST-235 model overestimates the path loss at 0.9 GHz and 2.4 GHz, while the Weissberger model underestimates the path loss. Among these models, the Multi-slope model demonstrates the highest accuracy for this data set: 6.7% (h_{Rx} = 2 m, 0.9 GHz) and 9.8% (h_{Rx} = 2 m, 2.4 GHz), as shown in Table 5, and 8.3% (h_{Rx} = 3.4 m, 0.9 GHz) and 12.2% (h_{Rx} = 3.4 m, 2.4 GHz), as shown in Table 6, respectively. Also, Figure 10 shows that the COST-235 model is appropriate for h_{Tx} λ/3 m to h_{Rx} 2 m and 3.4 m scenarios with co-polarized V-V antennas.

Figures 11 and 12 illustrate the comparison between predictions of the Weissberger, COST-235, and Multi-slope models and measured losses at the above-ground installation of the sensor node in the corn field, i.e., for a transmitting antenna height of 0.5 m at two frequencies (0.9 GHz and 2.4 GHz) and two receiving antenna heights (2.0 m and 3.4 m) for H-H (Figure 11) and V-V (Figure 12) polarized antennas. We can observe from Figure 11 and Tables 5 and 6 that the Weissberger model provides the best results in scenarios of above-ground installation of a sensor node in the cornfield at co-polarized H-H antennas, giving MAPE values of 6.4% and 12.7% for h_{Rx} = 2 m at 0.9 GHz and 2.4 GHz (Table 5) and of 6.2% and 7.5% for h_{Rx} = 3.4 m at 0.9 GHz and 2.4 GHz (Table 6), respectively. Also, Figure 12 shows that the COST-235 model is appropriate for h_{Tx} 0.5 m to h_{Rx} 2 m and 3.4 m scenarios with co-polarized V-V antennas.

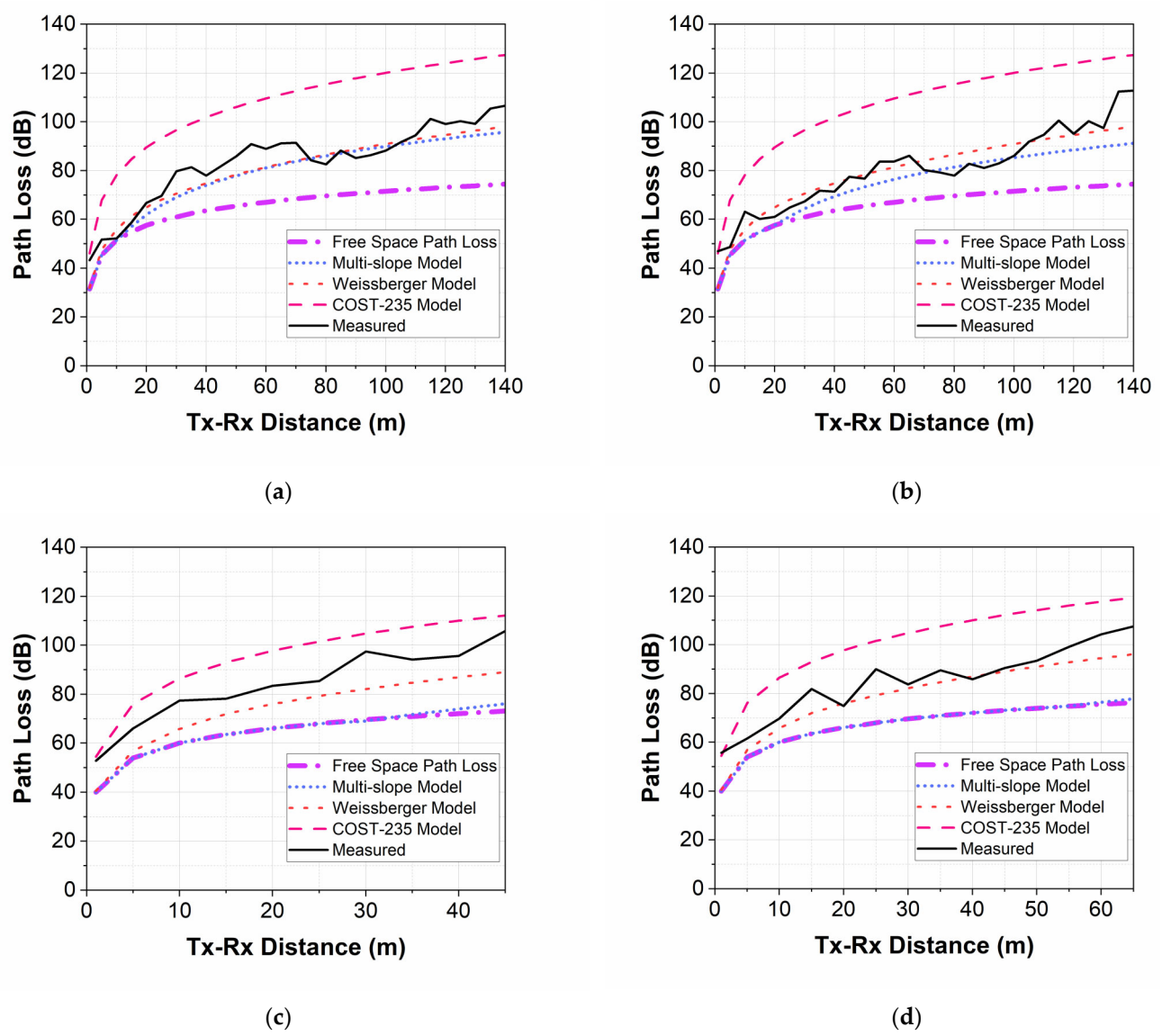

Figure 11. Comparison between losses for co-polarized H-H antennas at transmitting antenna height 0.5 m with existing models: (**a**) 0.9 GHz, h_{Rx} = 2.0 m; (**b**) 0.9 GHz, h_{Rx} = 3.4 m; (**c**) 2.4 GHz, h_{Rx} = 2.0 m; (**d**) 2.4 GHz, h_{Rx} = 3.4 m.

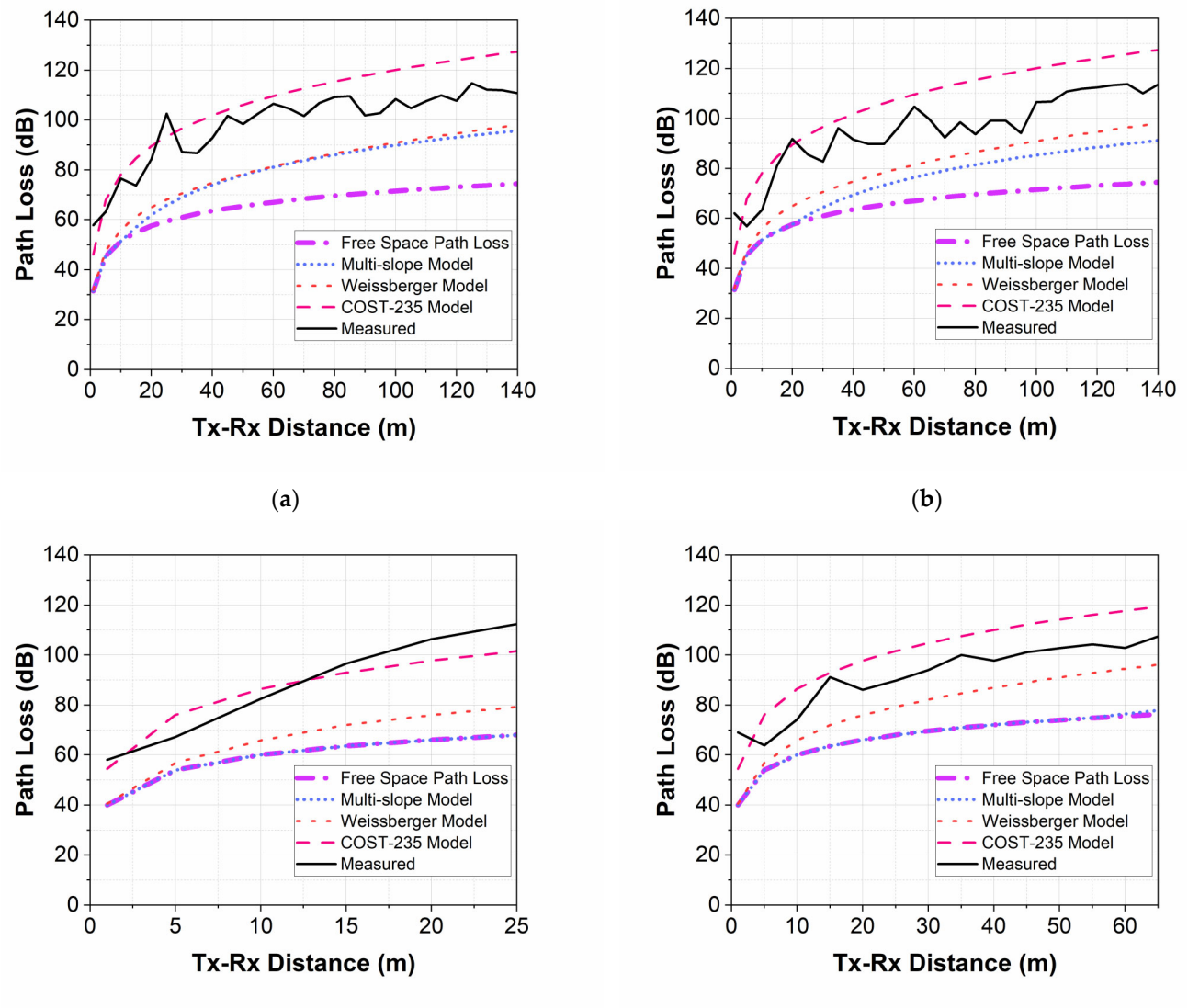

Figure 12. Comparison between losses for co-polarized V-V antennas at transmitting antenna height 0.5 m with existing models: (**a**) 0.9 GHz, h_{Rx} = 2.0 m; (**b**) 0.9 GHz, h_{Rx} = 3.4 m; (**c**) 2.4 GHz, h_{Rx} = 2.0 m; (**d**) 2.4 GHz, h_{Rx} = 3.4 m.

Table 5. A comparison of the mean absolute percentage error of Weissberger, COST-235, and Multi-slope models when they are used to predict the loss-versus-distance trend in several scenarios in a corn field at a receiving antenna height of 2 m.

h_{Rx} *	h_{Tx} *	Frequency **	Polarization ***	Mean Absolute Percentage Error			
				Basic Free-Space Loss	Multi-Slope Model	Weissberger Model	COST-235 Model
2	λ/3	0.9	H	26.7	6.7	14.4	16.8
		2.4	H	24.3	9.8	14.4	12.3
		0.9	V	36.7	15.3	25.8	3.9
		2.4	V	33.1	17.8	24.3	5.9
	0.5	0.9	H	20.9	7.2	6.4	28.6
		2.4	H	23.4	22.9	12.7	12.8
		0.9	V	33.6	20.9	19.4	10.2
		2.4	V	31.6	31.6	24.9	7.62

* h_{Rx} and h_{Tx} are receiving and transmitting antenna heights in meters. ** The frequency indicated in the table is in GHz. *** H—horizontal and V—vertical polarization.

Table 6. A comparison of the mean absolute percentage errors of Weissberger, COST-235, and Multi-slope models when they are used to predict the loss-versus-distance trend in several scenarios in a corn field at a receiving antenna height of 3.4 m.

h_{Rx} *	h_{Tx} *	Frequency **	Polarization ***	Mean Absolute Percentage Error			
				Basic Free-Space Loss	Multi-Slope Model	Weissberger Model	COST-235 Model
3.4	λ/3	0.9	H	24.4	8.3	10.6	22.9
		2.4	H	25.2	12.2	14.8	13.5
		0.9	V	33.8	14.7	21.0	9.4
		2.4	V	32.4	20.2	22.7	5.7
	0.5	0.9	H	17.9	8.2	6.2	33.7
		2.4	H	20.6	20.4	7.5	19.1
		0.9	V	31.34	22.2	16.6	14.0
		2.4	V	26.8	26.6	14.3	12.6

* h_{Rx} and h_{Tx} are receiving and transmitting antenna heights in meters. ** The frequency indicated in the table is in GHz. *** H—horizontal and V—vertical polarization.

We can conclude that the COST-235 model provides a reasonable estimate of the path loss of vertically polarized signals in corn fields, with MAPE values of 3.9% to 14.0% between the prediction and the actual path loss value. Hence, it is appropriate to recommend using the COST-235 model for omnidirectional, in-azimuth-plane vertical polarized antennas of nodes and base stations in both scenarios: near- and above-ground installation of sensor nodes in corn fields for smart agriculture. Also, concerning smart agriculture applications in the corn fields, the Multi-slope model performed well in the near-ground application scenarios at omnidirectional in-elevation-plane antennas with horizontal polarization. In addition, we identify the Weissberger model as suitable for planning radio coverage in the cornfield for the above-ground node connectivity scenario with omnidirectional in-elevation plane and horizontal polarization.

4. Future Work

The results of this work also provide a foundation for future work in radio wave propagation in the vegetation fields for smart agriculture communication scenarios. One area for future work is combining the knowledge gained about radio wave propagation in the corn field (R3 stage) with that without vegetation or in other corn growth stages. We also plan to examine how the x-polarization of the antennas will impact the coverage area of a wireless sensor network for IoT-based smart agriculture. Another area involves performing a measurement campaign collecting received signal-strength indicator (RSSI) and packet loss from sensors (from a wireless sensor network) placed at the same position as the transmitting antenna.

5. Conclusions

This study examines the influence of vegetation on radio wave propagation in real-world scenarios for IoT-based smart agriculture applications in a corn field at 0.9 GHz and 2.4 GHz. All measurements were conducted in a corn field at stage R3, during which the corn leaves and stalk almost do not change and the kernels contain approximately 80% moisture. The results indicate that increasing the receiving antenna height above the corn height, from 2.0 m to 3.4 m, expanded the coverage area. The maximum communication distance for near-ground installation of the sensor node (where the transmitter is λ/3 m above ground) in a corn field, with a base station (receiving) antenna height of 3.4 m, was found to be 105 m at 0.9 GHz and 45 m at 2.4 GHz in the obstructed line-of-sight (O-LoS) scenario for co-polarized H-H antennas. Moreover, a more significant increase in the communication distance between the transmitting and receiving antennas was observed when the transmitting antenna height was increased from λ/3 m (0.11 m at 0.9 GHz and 0.04 m at 2.4 GHz) to 0.5 m above ground level. The maximum communication distance for above-ground installation of the sensor node (0.5 m above ground) in a corn field, with a base station antenna height of 3.4 m, was found to be 140 m at 0.9 GHz

and 65 m at 2.4 GHz in the O-LoS scenario for co-polarized H-H antennas. Also, the results show that, for vertical polarization Tx-Rx antennas, the received signal experienced higher attenuation than for horizontal ones, especially at 0.9 GHz. In contrast, at 2.4 GHz, antenna polarization had minimal impact on the coverage area. In addition, we identify the three models suitable for planning radio coverage in a cornfield in the following scenarios: (1) Multi-slope model for the near-ground node connectivity scenario with omnidirectional in-elevation-plane antennas and horizontal polarization; (2) Weissberger model for above-ground node connectivity scenario with omnidirectional in-elevation-plane antennas and horizontal polarization; and (3) COST-235 model for omnidirectional in-azimuth-plane vertical polarized antennas of nodes and base stations in both near- and above-ground scenarios.

This work provides insights into radio wave propagation in a corn field in different scenarios, making it suitable for radio coverage planning in the presence of crops where plants are grown in rows with vertically oriented stalks (such as corn, sunflower, etc.) to ensure reliable and resilient wireless communications in IoT-based smart agriculture.

Author Contributions: Conceptualization, B.N.A., N.T.A. and G.L.A.; methodology, B.N.A., N.T.A. and G.L.A.; software, N.T.A. and B.N.A.; validation, B.N.A., N.T.A. and G.L.A.; formal analysis, N.T.A. and G.L.A.; investigation, B.N.A., N.T.A. and G.L.A.; resources, N.T.A. and G.L.A.; data curation B.N.A., N.T.A. and G.L.A.; writing—original draft preparation, B.N.A. and G.L.A.; writing—review and editing, B.N.A. and N.T.A.; visualization, B.N.A. and N.T.A.; supervision, N.T.A.; project administration, N.T.A.; funding acquisition, N.T.A. and G.L.A. All authors have read and agreed to the published version of the manuscript.

Funding: This research was funded by the BULGARIAN NATIONAL SCIENCE FUND at the Ministry of Education and Science, Bulgaria, grant number KP-06-H67/4 from 12th December 2022 "Development and testing of new models of radio channels and antennas for reliable and resilient wireless connectivity enabling innovative applications in future IoT-based precision agriculture".

Data Availability Statement: The data presented in this study are available upon request from the authors.

Conflicts of Interest: The authors declare no conflicts of interest.

References

1. *World Population Prospects 2022 Summary of Results*; United Nations: New York, NY, USA, 2022.
2. Cama-Pinto, D.; Damas, M.; Holgado-Terriza, J.A.; Arrabal-Campos, F.M.; Martínez-Lao, J.A.; Cama-Pinto, A.; Manzano-Agugliaro, F.A. Deep learning model of radio wave propagation for precision agriculture and sensor system in greenhouses. *Agronomy* **2023**, *13*, 244. [CrossRef]
3. Gopalakrishnan, S.; Waimin, J.; Zareei, A.; Sedaghat, S.; Raghunathan, N.; Shakouri, A.; Rahimi, R. A biodegradable chipless sensor for wireless subsoil health monitoring. *Sci. Rep.* **2022**, *12*, 8011. [CrossRef]
4. Kakamoukas, G.; Sarigiannidis, P.; Maropoulos, A.; Lagkas, T.; Zaralis, K.; Karaiskou, C. Towards climate smart farming—A reference architecture for integrated farming systems. *Telecom* **2021**, *2*, 52–74. [CrossRef]
5. Jägermeyr, J.; Müller, C.; Ruane, A.C.; Elliot, J.; Balkovic, J.; Castillo, O.; Faye, B.; Foster, I.; Folberth, C.; Franke, J.A.; et al. Climate impacts on global agriculture emerge earlier in new generation of climate and crop models. *Nat. Food* **2021**, *2*, 873–885. [CrossRef]
6. Atanasov, N.T.; Atanasov, B.N.; Atanasova, G.L. Flexible wearable antenna for IoT-based plant health monitoring. *Electronics* **2024**, *13*, 2956. [CrossRef]
7. Kurrer, C.; Tarlton, J. Ten More Technologies Which Could Change Our Lives. In-Depth Analysis. STOA, European Union: Brussels, Belgium, 2017. Available online: https://www.europarl.europa.eu/thinktank/en/document/EPRS_IDA(2017)598626 (accessed on 14 July 2017).
8. Tomaszewski, L.; Kołakowski, R. Mobile services for smart agriculture and forestry, biodiversity monitoring, and water management: Challenges for 5G/6G networks. *Telecom* **2023**, *4*, 67–99. [CrossRef]
9. Novak, H.; Ratković, M.; Cahun, M.; Lešić, V. An IoT-based encapsulated design system for rapid model identification of plant development. *Telecom* **2022**, *3*, 70–85. [CrossRef]
10. Di Tocco, J.; Lo Presti, D.; Massaroni, C.; Cinti, S.; Cimini, S.; De Gara, L.; Schena, E. Plant-Wear: A multi-sensor plant wearable platform for growth and microclimate monitoring. *Sensors* **2023**, *23*, 549. [CrossRef]
11. Chenniappan, P.; Ramalingam, K.; Pazhanivelan, S.; Kaliaperumal, R. Smart farming: Internet of Things (IoT)-based sustainable agriculture. *Agriculture* **2022**, *12*, 1745. [CrossRef]

12. Hakim, G.P.N.; Habaebi, M.H.; Toha, S.F.; Islam, M.R.; Yusoff, S.H.B.; Adesta, E.Y.T.; Anzum, R. Near ground pathloss propagation model using adaptive neuro fuzzy inference system for wireless sensor network communication in forest, jungle and open dirt road environments. *Sensors* **2022**, *22*, 3267. [CrossRef]
13. Et-taibi, B.; Abid, M.R.; Boufounas, E.-M.; Morchid, A.; Bourhnane, S.; Hamed, T.A.; Benhaddou, D. Enhancing water management in smart agriculture: A cloud and IoT-Based smart irrigation system. *Engineering* **2024**, *22*, 102283. [CrossRef]
14. Checco, A.; Fabiani, V.; Palmisano, M.; Polese, D. Network connectivity and sensor response of an OpenThread WSN platform for crop monitoring. *IEEE Trans. AgriFood Electron.* **2024**, *2*, 218–225. [CrossRef]
15. *Applications of Wireless Sensor Networks in Next Generation Networks*; ITU-T, International Telecommunication Union: Geneva, Switzerland, 2014.
16. Hidalgo-Leon, R.; Urquizo, J.; Silva, C.E.; Silva-Leon, J.; Wu, J.; Singh, P.; Soriano, G. Powering nodes of wireless sensor networks with energy harvesters for intelligent buildings: A review. *Energy Rep.* **2022**, *8*, 3809–3826. [CrossRef]
17. Quy, V.K.; Hau, N.V.; Anh, D.V.; Quy, N.M.; Ban, N.T.; Lanza, S.; Randazzo, G.; Muzirafuti, A. IoT-enabled smart agriculture: Architecture, applications, and challenges. *Appl. Sci.* **2022**, *12*, 3396. [CrossRef]
18. Muangprathub, J.; Boonnam, N.; Kajornkasirat, S.; Lekbangpong, N.; Wanichsombat, A.; Nillaor, P. IoT and agriculture data analysis for smart farm. *Comput. Electron. Agric.* **2019**, *156*, 467–474. [CrossRef]
19. Temene, N.; Sergiou, C.; Ioannou, C.; Georgiou, C.; Vassiliou, V. A node placement algorithm utilizing mobile nodes in WSN and IoT networks. *Telecom* **2022**, *3*, 17–51. [CrossRef]
20. Gao, Z.; Li, W.; Zhu, Y.; Tian, Y.; Pang, F.; Cao, W.; Ni, J. Wireless channel propagation characteristics and modeling research in rice field sensor networks. *Sensors* **2018**, *18*, 3116. [CrossRef]
21. Zhang, H.; Zhang, J. Path loss modeling for 2.4 GHz wireless channel in wheat fields. *Trans. Chin. Soc. Agric. Mach.* **2014**, *45*, 291–296.
22. Li, Z.; Wang, N.; Hong, T. Radio path-loss modeling for a 2.4 GHz in-field wireless sensor network. *Trans. ASABE* **2010**, *53*, 615–624. [CrossRef]
23. Rizky, R.; Mustafid; Mantoro, T. Improved performance on wireless sensors network using multi-channel clustering hierarchy. *J. Sens. Actuator Netw.* **2022**, *11*, 73. [CrossRef]
24. Li, H.; Wang, N. Radio propagation characteristics of 2.4 GHz at specific growth stages of corn. In Proceedings of the 2013 ASABE Annual International Meeting, Kansas City, MI, USA, 21–24 July 2013.
25. Li, F.; Wu, H.; Miao, Y.; Zhu, L. A research on the radio signal propagation characteristics in corn field. *BTAIJ* **2013**, *8*, 1347–1352.
26. Mohsen, M.; Matolak, D.W. Vegetation attenuation for several evergreen shrubs at 31 and 5 GHz. In Proceedings of the 2018 11th Global Symposium on Millimeter Waves (GSMM), Boulder, CO, USA, 22–24 May 2018.
27. Navarro, A.; Guevara, D.; Florez, G.A. An adjusted propagation model for wireless sensor networks in corn fields. In Proceedings of the URSI GASS 2020, Rome, Italy, 29 August–5 September 2020.
28. Tang, W.; Ma, X.; Wei, J.; Wang, Z. Measurement and analysis of near-ground propagation models under different terrains for wireless sensor networks. *Sensors* **2019**, *19*, 1901. [CrossRef] [PubMed]
29. Al-Sehemi, A.; Al-Ghamdi, A.; Dishovsky, N.; Atanasova, G.; Atanasov, N. A flexible broadband antenna for IoT applications. *Int. J. Microw. Wirel. Technol.* **2020**, *12*, 531–540. [CrossRef]
30. Development Guide: NB-IoT for Agriculture, GSMA, 5 October 2018. Available online: https://www.gsma.com/solutions-and-impact/technologies/internet-of-things/gsma_resources/guide2-nbiot-agriculture/ (accessed on 5 October 2018).
31. Valecce, G.; Petruzzi, P.; Strazzella, S.; Grieco, L.A. NB-IoT for smart agriculture: Experiments from the field. In Proceedings of the 2020 7th International Conference on Control, Decision and Information Technologies (CoDIT'20), Prague, Czech Republic, 29 June–2 July 2020.
32. Sokullu, R. LoRa based smart agriculture network. In Proceedings of the 2022 8th International Conference on Energy Efficiency and Agricultural Engineering (EE&AE), Ruse, Bulgaria, 30 June–2 July 2022.
33. Ramos, B.; del Rosario, E.; Tovar, N. Analysis of LoRa signal characteristics at maize and cocoa crops in tropical regions. In Proceedings of the 2023 IEEE-APS Topical Conference on Antennas and Propagation in Wireless Communications (APWC), Venice, Italy, 9–13 October 2023.
34. Mowla, M.N.; Mowla, N.; Shah, A.F.M.S.; Rabie, K.M.; Shongwe, T. Internet of Things and wireless sensor networks for smart agriculture applications: A survey. *IEEE Access* **2023**, *11*, 145813–145852. [CrossRef]
35. KNOX County Agricultural News OSU Extention. Available online: https://u.osu.edu/knoxcountyag/2019/08/ (accessed on 23 August 2019).
36. Nleya, T.; Chungu, C.; Kleinjan, J. *Corn Growth and Development*; North Dakota State University: Bismarck, ND, USA, 2019; pp. 5–8.
37. Plumblee, M.; Harrelson, B.; Halladay, S. Visual Guide to Corn Growth Stages. Land-Grant Press by Clemson Extension: Clemson, SC, USA, 2023; LGP 1170.
38. World Economic Forum. Available online: https://www.weforum.org/agenda/2021/06/corn-industries-sustainability-food-prices/ (accessed on 2 June 2021).
39. Wang, J.; Hu, X. Research on corn production efficiency and influencing factors of typical farms: Based on data from 12 cornproducing countries from 2012 to 2019. *PLoS ONE* **2021**, *16*, e0254423. [CrossRef]

40. *IEC/IEEE 62209-1528:2020*; IEC/IEEE International Standard-Measurement Procedure for the Assessment of Specific Absorption Rate of Human Exposure to Radio Frequency Fields from Hand-Held and Body-Mounted Wireless Communication Devices—Part 1528: Human Models, Instrumentation, and Procedures (Frequency Range of 4 MHz to 10 GHz). IEEE: New York, NY, USA, 2020.
41. Neelam, M.; Mohanty, B.P. On the radiative transfer model for soil moisture across space, time and hydro-climates. *Remote Sens.* **2020**, *12*, 2645. [CrossRef]
42. Barclay, L. *Propagation of Radiowaves*, 3rd ed.; The Institution of Engineering and Technology: London, UK, 2013; pp. 308–310.
43. Barrios-Ulloa, A.; Ariza-Colpas, P.P.; Sánchez-Moreno, H.; Quintero-Linero, A.P.; De la Hoz-Franco, E. Modeling radio wave propagation for wireless sensor networks in vegetated environments: A systematic literature review. *Sensors* **2022**, *22*, 5285. [CrossRef]
44. Seybold, J.S. *Introduction to RF Propagation*; John Wiley & Sons: Hoboken, NJ, USA, 2005; pp. 134–162.
45. De Beelde, B.; De Beelde, R.; Tanghe, E.; Plets, D.; Verheyen, K.; Joseph, W. Vegetation loss at D-Band frequencies and new vegetation-dependent exponential decay model. *IEEE Trans. Antennas Propag.* **2022**, *70*, 12092–12103. [CrossRef]
46. *Calculation of Free-Space Attenuation*; ITU-R, International Telecommunication Union: Geneva, Switzerland, 2019.